6. STRONG METAL-SUPPORT INTERACTIONS (SMSI)

It has long been recognized that the efficiency of a supported catalyst is strongly related to the extent of metal dispersion and metal-support interactions. The search for better dispersion and supports has contributed diverse catalyst synthesis techniques and a variety of support materials. Today, discussion of the topics related to metal dispersion and metal-support interaction is becoming increasingly common and sophisticated, thanks in large part to advances in analytical techniques. As evidenced by the increasing acceptance of the acronym SMSI (strong metal-support interactions), the subject is no longer a vague awareness but is firmly established as an area of catalysis with important practical implications. SMSI has recently been the theme of a conference (32) and a multiclient study (33). This section presents an overview of SMSI with examples of diverse applications, including Fischer-Tropsch synthesis.

6.1 GENERAL CHARACTERIZATION

Advances have been made in many related areas of metal-support interactions. Evidence is emerging that metal-support interactions are widespread phenomena that differ in strength. This is influenced by three key properties of the interacting metal supports:

- Energetics of metal particles--the properties reflecting the cohesive energy of a particle
- Geometric properties--those describing shape, size, crystal habit, order, strain, and structure
- Electronic properties--those describing the band structure, electron binding energies, and interactions of electrons with magnetic fields.

As the research expands, some authors feel it necessary to separate the metal-support interactions into three categories: weak (WMSI), medium (MMSI), and strong (SMSI) (32). The allocation of various interactions to each of these categories is somewhat arbitrary at this time, but it is generally accepted that metals on oxides such as SiO_2, Al_2O_3, and MgO, as well as carbon or graphite, show WMSI (exceptions may exist when the oxide supports are subjected to very high reduction temperatures); small metal particles in zeolites show MMSI; and metals on certain reducible oxides (especially TiO_2) show SMSI. SMSI is the largest category.

The main requirements of SMSI are the presence in the support surface of a local anion deficiency that allows the metal atoms (cluster) and the reduced center to approach closely (53), and a metal ion of lower than normal oxidation number, generated by partial reduction of the support surface (35, 41). The occurrence of SMSI correlates with the reducibility of the oxide support. Thus, no SMSI effect is found when alumina (Al_2O_3), silica (SiO_2), magnesia (MgO), scandia (Sc_2O_3), hafnia (HfO_2), zirconia (ZrO_2), or yttria (Y_2O_3) are reduced at 770K in hydrogen. All are very resistant to reduction, with equilibrium values of P_{H_2O}/P_{H_2} at 1000K being less than 10-13. On the other hand, the SMSI effect is observed with the more easily reducible oxides such as titania (TiO_2), tantala (Ta_2O_5), niobia (Nb_2O_5), vanadium oxide (V_2O_3), and manganese oxide (MnO). For titania, the effect has been directly correlated with the occurrence of Ti^{3+} ions in the support surface. There is little doubt that with other active supports, superficial reduction is also responsible for inducing the SMSI effect with other active supports. If the reduction temperature is low--about 470K, for example--essentially no effect is observed. This correlates with an absence of surface reduction of the support.

SMSI has been observed with cluster dispersions of most of the Group VIII metals--platinum, iridium, osmium, palladium, rhodium, and ruthenium. The consequences of this metal-support interaction can be considerable. SMSI greatly influences the extent of hydrogen and carbon monoxide absorption. Also, electron microscopic evidence suggests that the strength of the interaction between the metal and the support induces the metallic cluster to adopt a raft-like morphology that maximizes the number of metal atoms in contact with the support.

This changed morphology may have catalytic consequences quite apart from the electronic interaction, because a changed morphology changes the nature of the exposed crystal facets. In particular, the raft-like morphology in the SMSI state should increase the proportion of low-index planes and may even result in only a single low-index plane being present.

Because SMSI is due to interaction of the cluster with ions of lower valency in the support surface, the effect should be reversible upon oxidation. Experimental evidence supports this. Treatment in oxygen, typically at 770K, converts the SMSI state to one that, when reduced in hydrogen at low temperatures (470K), exhibits normal chemisorption behavior.

It is interesting to note that both SMSI (electron-rich clusters) and reduced metals associated with molybdenum or tungsten centers (electron-deficient clusters) lead to reduced uptake of hydrogen and carbon monoxide. This implies the existence of an optimum situation between these limits with respect to these absorption processes, although the implications for absorption theory have not yet been evaluated.

As stated above, the SMSI phenomenon results in a metallic cluster that tends to adopt a raft-like morphology on the support surface. No data are yet available for multimetallic clusters on supports that exhibit SMSI. For platinum-gold particles dispersed on silica or γ-alumina (non-SMSI supports), the different strengths with which platinum and gold interact with the support could probably lead to phase separation (54). This effect is dependent both on the nature of the support and on the gaseous environment. When a γ-alumina support is heated in oxygen at 720K, a phase separation of platinum-gold clusters results because of the strong interaction of oxygen-covered platinum with the γ-alumina surface. This does not occur when a silica support is used, presumably because the platinum-silica interaction is comparable to gold-silica. These conclusions are drawn primarily from experimental data on hydrocarbon reactivity.

For a silica-supported platinum-palladium dispersion, treatment in oxygen (air), followed by hydrogen reduction, can lead to phase separation (55, 56). Phase separation caused by different strengths of interaction of the metallic

components with the support is an important, and probably widespread, phenomenon in supported multimetallic systems. Such a phase separation must always be considered when discussing catalytic activity and is deserving of more study.

In principle, metal-support interactions provide yet another parameter for modifying the physical and chemical properties of multimetallic systems in the search for improved catalysts. Modification of the electron concentration and distribution within the cluster appears feasible. Such modifications may, in fact, profoundly affect the nature of the interaction between metals in small clusters by influencing surface composition or the miscibility of the metals. The stabilization of raft-like structures is also expected to influence the catalytic properties of multimetallic catalysts on strongly interacting supports.

6.2 HYDROGEN CHEMISORPTION UNDER SMSI

Hydrogen chemisorption to characterize supported catalysts is widely practiced because it gives a precise measure of the dispersion of the metal, since each surface metal atom chemisorbs a single hydrogen atom. Thus, when the cross section for the adsorbed hydrogen atom is known, the surface area of the exposed metal on which the chemical reaction occurs can be determined.

Investigations into the phenomena of SMSI, however, have uncovered an anomaly in this practice. For example, hydrogen adsorption on titania-supported noble metal catalysts has been measured, and it was found that where SMSI occurs, hydrogen chemisorption is not a reliable means of measuring the metal surface area (35). The results of this study are shown in Table 6-1.

The values in Table 6-1 are expressed as the number of hydrogen atoms adsorbed per total number of metal atoms on the support. The adsorption was done at 25°C after the catalyst samples had been reduced in situ under H_2 flow at 200°C and 500°C.

Table 6-1

Hydrogen Chemisorption on TiO_2-Supported Group VIII Noble Metals

Metal, wt%	Ratio of Hydrogen Atoms Adsorbed to Total Metal Atoms	
	Reduction at 200°C	Reduction at 500°C
Ruthenium	0.23	0.06
Rhodium	0.71	0.01
Palladium	0.93	0.05
Osmium	0.21	0.11
Iridium	1.60	0.00
Platinum	0.88	0.00

Reference: (35)

The samples reduced at 200°C exhibit hydrogen chemisorption properties typical of the corresponding well-reduced metals on familiar supports such as alumina or silica. Those reduced at 500°C, however, lose much of their chemisorption capacity.

X-ray diffraction and electron microscopy of the samples listed in Table 6-1 showed that the metal dispersion remained high for both batches of samples. Therefore, metal agglomeration at 500°C could not have accounted for the reduced chemisorption capabilities. The possibility that low chemisorption results from encapsulation of metal particles by the support due to structural collapse was ruled out by measurement of the total surface area, which showed no such collapse.

The conclusion of this study was that Group VIII noble metals dispersed on titania exhibit normal affinity toward hydrogen if they are on typical supports such as aluminia or silica, and if the reduction temperature is kept low. Hydrogen reduction of these catalysts at 500°C converts the metals to a drastically altered state and reduces the hydrogen affinity dramatically, despite the fact that the metals remain well dispersed.

Ir is one of the Group VIII noble metals that shows pronounced SMSI with TiO_2 (Table 6-1). Using H_2 chemisorption, another study compared the SMSI of transition metal oxide supports plus MgO with Ir (41). The objective of the study was to see if a correlation exists between the SMSI of oxides and their reducibility. Table 6-2 lists the properties of the supports.

H_2 chemisorption was measured after the supports were reduced in H_2 at temperatures ranging from 120°C to 700°C. Figure 6-1 shows the data expressed as the logarithm of hydrogen atoms adsorbed per atom of iridium on the support versus the reduction temperature. This figure clearly separates one group of oxides that is relatively unaffected by the reduction temperature from a second group that is significantly affected. The two groups are as follows:

Table 6-2

Support Properties of the SMSI of Oxides

	BET Area, m^2/g	Ir, wt%
Magnesium oxide, MgO	31	2
Scandium oxide, Sc_2O_3	70	2
Yttrium oxide, Y_2O_3	54	2
Titanium oxide, TiO_2	145	2
Zirconium oxide, ZrO_2	41	2
Hafnium oxide, HfO_2	-	1
Vanadium oxide, V_2O_3	6.7	1
Niobium oxide, Nb_2O_5	26	2
Tantalum oxide, Ta_2O_5	135	2

Reference: (41)

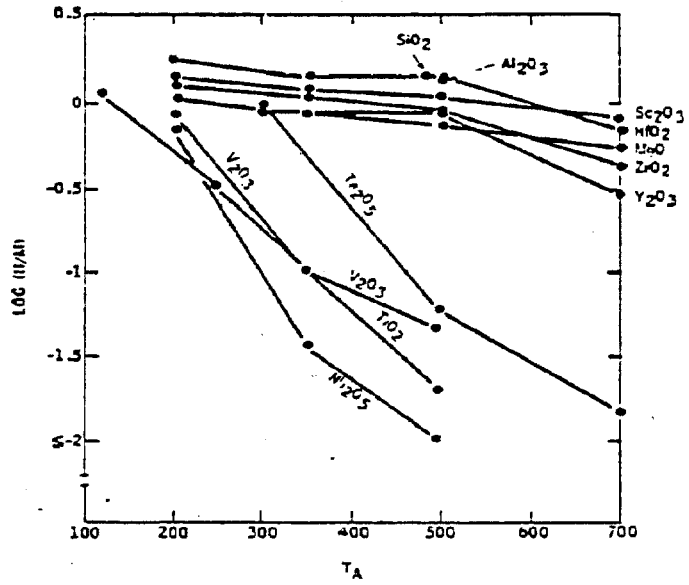

Figure 6-1. H_2 Chemisorption versus Temperature of Activation for Supported Iridium Catalysts. H/M = atoms hydrogen adsorbed at 25°C per atom iridium present in catalysts; T_A = temperature of activation in hydrogen; wt% iridium = 1 for SiO_2, Al_2O_3, V_2O_3, and HfO_2; wt% iridium = 2 for all other catalysts.

Reference: (41)

SMSI	Non-SMSI
TiO_2	MgO
V_2O_3	Sc_2O_3
Nb_2O_5	Y_2O_3
Ta_2O_5	ZrO_2
	HfO_3

The chemical formulas are those of the bulk phases as indicated by x-ray inspection of the catalysts at the conclusion of the H_2 chemisorption measurements. The surface compositions, especially for the SMSI supports, may be different.

To find what causes the SMSI, the authors arranged the saturated transition metal oxides in order of decreasing resistance to reduction. A saturated oxide is one whose cation formally has zero d-orbital occupancy. This leads to the finding that V_2O_3 is the only exception among the transition metal oxides in this study.

The reducibility of an oxide can be expressed as the logarithm of the ratio P_{H_2O}/P_{H_2} as the oxide comes to an equilibrium in the relation:

$$\text{oxide} + H_2 \longrightarrow \text{reduced state} + H_2O \qquad (6.1)$$

The reducibility of the oxides in the study at 1000K (727°C) is listed, along with the SMSI activities, in Table 6-3.

Among the oxides that show positive SMSI (Figure 6-1), the SMSI activity correlates well with the reducibility parameter. Nb_2O_5 shows the greatest SMSI and the least resistivity to reduction. Ta_2O_5 is least active in SMSI and the most resistive to reduction. TiO_2 has intermediate values.

Recently, Baker has studied H_2 chemisorption for Ni supported on graphite and has found some anomalies resembling SMSI (46). The catalyst, comprised of 2.7 wt% Ni on graphite foil, was treated in the sequence described in Table 6-4.

Table 6-3

Correlation of SMSI Properties with Reducibility for Saturated Transition Metal Oxides

Oxide	Reduced State	Reducibility log [P_{H_2O}/P_{H_2}] at 1000K	SMSI Activity
Sc_2O_3	Sc	-18.1	Negative
Y_2O_3	Y	-18.0	Negative
HfO_2	Hf	-14.0	Negative
ZrO_2	Zr	-13.6	Negative
Ta_2O_5	Ta	-6.8	Positive
TiO_2	Ti_3O_5	-3.9	Positive
Nb_2O_5	NbO_2	-1.1	Positive

Reference: (41)

Table 6-4

Reduction and Reaction Conditions for Ni-Graphite (Grafoil) Catalysts[a]

Treatment	Temperature, K	Time, h	Gas Environment	Remarks
1	870 - 1150	1-2	Hydrogen	Reduction
	820	0.5	-	Evacuation
	295	0.25	-	Evacuation (FMR, H_2 chemisorption)
1'	295	0.5	-	Evacuation (H_2 chemisorption)
2	1320	0.5-2	Hydrogen	Spreading of nickel
	820	0.5	-	Evacuation
	295	0.25	-	Evacuation (FMR, H_2 chemisorption)
2'	295	0.25	-	Evacuation (H_2 chemisorption)
3	1100 - 1320	1.0	Water and helium	Steaming $He:H_2O$ = 35:1
	570	0.25	Helium	Flush
	295	0.25		Evacuation (FMR, H_2 chemisorption)

[a]Consecutive treatments

Reference: (46)

Figure 6-2 shows the H_2 chemisorption in each treatment (identified by the treatment number). The transformations from treatments 1 through 3 in Figure 6-2 were observed by controlled atmosphere electron microscopy (CAEM) (see Section 7.4). CAEM uses a high-resolution transmission electron micoscope with about 2.5-nm resolution. Its unique design permits the observation of samples under reaction conditions. In this study, Ni particles under 1 torr of H_2 pressure were observed at various temperatures. The nucleation started at 1030K.

Catalytic attack of the substrate commenced at 1120K, resulting in fine channels having Ni particles at their leading edges. As the temperature was raised to 1250K, Ni particles tended to undergo periodic shape rearrangements, as noticed from changes in the shape of the meniscus at their trailing edges. At 1320K, a gradual depletion in the size of the particles occurred until ultimately all the catalyst was depleted and the channeling ceased.

In Figure 6-2, curve 1 (1150K) and curve 2 (1320K) reflect the morphological changes occurring to Ni. Ferromagnetic resonance measurements indicate that at high temperatures Ni is deposited as a thin film along the channel walls. The failure to observe the Ni film by CAEM indicates that the film is less than 2.5 nm thick, the resolution of the CAEM.

At high temperatures, when atomic mobility is present, the metal disperses over the substrate as a thin film if the metal-support interaction dominates the metal cohesion energy (45, 47, 48). This seems to be what is happening for Ni on carbon at >1250K.

6.3 CO CHEMISORPTION UNDER SMSI

CO chemisorption is also used to characterize surface metal. It was demonstrated by the study cited in Section 6.1 (35) that where SMSI affects the hydrogen chemisorption, it also affects CO chemisorption (Table 6-5). The catalyst samples reduced at 200°C exhibit CO adsorption capacities similar to those supported on alumina or silica. As with hydrogen, high-temperature reduction drastically reduces the CO affinity.

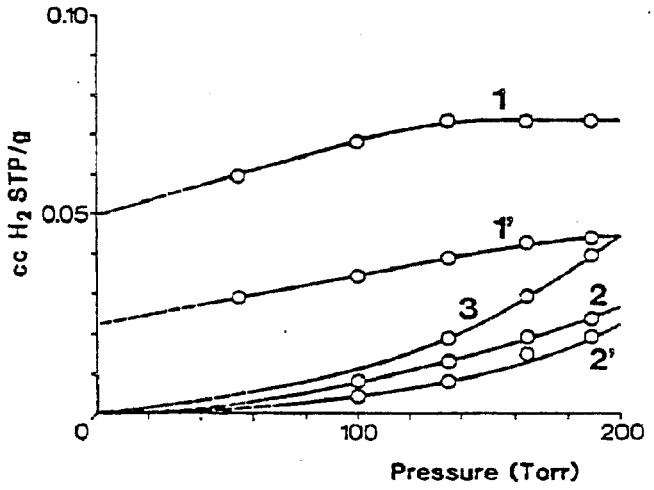

Figure 6-2. Hydrogen Chemisorption Isotherms (295K) of a 2.7 wt% Ni-Grafoil Catalyst Following the Pretreatments Described in Table 6-4

Reference: (46)

Table 6-5

Carbon Monoxide Chemisorption on TiO_2-Supported Group VIII Noble Metals

Metal, 2 wt%	Ratio of Carbon Monoxide Molecules Adsorbed to Total Metal Atoms: Reduction at 200°C	Reduction at 500°C
Ruthenium	0.64	0.11
Rhodium	1.15	0.02
Palladium	0.53	0.02
Iridium	1.19	0.00
Platinum	0.65	0.03

6.4 REVERSIBILITY OF SMSI

Tauster (35) showed that reversible removal of the SMSI capacity of the Pd/TiO_2 can be achieved by oxygen treatment. SMSI of 2 wt% Pd capacity on TiO_2 (Table 6-1) was accomplished by high temperature reduction in H_2, followed by oxidation at 400°C in O_2. Reduction at a low temperature restored the H_2 chemisorption capacity. Subsequent high-temperature reduction restored SMSI. The sequence is summarized in Table 6-6.

Steam treatment also reverses SMSI. For example, Baker showed that Pt/TiO_2 under SMSI can be steam-treated, resulting in a restoration of the H_2 chemisorption capacity (49). A 2 wt% Pt/TiO_2 powder was treated under various conditions and was tested for H_2 and CO chemisorption. Table 6-7 shows the sequence of treatments and the chemisorption results.

After reduction at 425K (Step A), the fresh samples have normal adsorption capacities. Step B induces SMSI, as evidenced by the loss of chemisorption capabilities. Some recovery from SMSI is made in Step C when the sample is treated with steam at 525K. The recovery is greater for H_2 chemisorption than for CO chemisorption. Step D illustrates that O_2 is more efficient in restoring the chemisorption capacities than steam.

Transmission electron microscopy of the above specimens showed that after Step B Pt particles are in the form of hexagonal pillbox shapes (43). Oxidation by H_2O Transmission electron microscopy of the above specimens showed that after Step B Pt particles are in the form of hexagonal pillbox shapes (43). Oxidation by H_2O or O_2 produced some significant changes in the appearance and structure of the Pt particles. Oxidation caused an apparent increase in particle size. Close examination of individual particles showed that while in many cases they retained the hexagonal outline, they were no longer flat, especially after the O_2 treatment.

Examination by electron diffraction demonstrated that following Step B, the support had a structure corresponding to Ti_4O_7, whereas after both oxidation in steam and O_2, it was converted back to TiO_2.

Table 6-6

Reversibility of SMSI

Sample: 2 wt% Pd/TiO_2

Treatment in Sequence	H_2 Chemisorption, H Atoms/Metal Atom
Low-temperature reduction: H_2, 175°C	0.93
High-temperature reduction: H_2, 500°C	0.05
Oxidation: O_2, 400°C, 1 h	
Low-temperature reduction: H_2, 175°C	0.89
High-temperature reduction: H_2, 500°C	0.03

Reference: (35)

Table 6-7

Chemisorption of H_2 and CO on 2 wt% Pt/TiO_2

Treatments	Evacuation before Chemisorption	Chemisorption at Ambient Temperature	
		H Atoms/Pt Atom	CO Molecules/ Pt Atom
(A) H_2, 1 h, 425K	2 h, 425K	0.61	0.41
(B) H_2, 1 h, 875K	0.5 h, 725K	0	0
(C) H_2, 1 h, 875K H_2O (15 torr), 525K H_2, 1 h, 425K	2 h, 425K	0.13	0.09
(D) H_2, 1 h, 875K O_2, 1 h, 875K	1 h, 425K	0.39	0.26

Reference: (49)

Duprez studied H_2 generation from steam treatment of the metals Rh, Pt, and Ni in SMSI with TiO_2 (50). The catalysts, 0.23% Rh/TiO_2, 0.45% Pt/TiO_2, and 3.7% Ni/TiO_2, were prepared by wet impregnation of anatase (99% TiO_2, 8-10 m^2/g surface area). After calcination at 723K, one batch was reduced at 773K for 15 h under H_2, followed by flushing with Ar at 773K. The other batch was reduced at 473K for 15 h and then flushed with Ar for 3 h at 473K. The SMSI effect is evident in the high-temperature reduced samples.

H_2 chemisorption on these catalyst samples was carried out at 300K. The results are shown in Table 6-8. The SMSI effect is evident in the high-temperature reduced samples.

Subsequently, pulses of water vapor were passed over the reduced catalyst samples at 773K and the H_2 emerging from the catalyst was measured. The results are shown in Figure 6-3.

It has been established that high-temperature reduction, which induces SMSI of noble metals on TiO_2, eliminates the lattice oxygen ions and forms H_2O (51, 52). Baker noted that after reduction of Pt/TiO_2, the support was transformed to the oxide Ti_4O_7. It appears that high-temperature reduction leads to the formation of anion vacancies, leaving the solid with excess free electrons. From this evidence, Duprez proposed that hydrogen is produced by the reactions

$$2\ e^- + \text{Vacancy} + H_2O \longrightarrow O^{-2} + H_2(g) \qquad (6.2)$$

or

$$2\ Ti^{+3} + H_2O \longrightarrow 2\ Ti^{+4} + O^{-2} + H_2(g) \qquad (6.3)$$

In Figure 6.3b it is interesting that some H_2 generation is measured from samples reduced at 473K. It may be possible that some reduction of the support occurred when the catalysts were reduced for very long periods (15 h). In the original SMSI work by Tauster, the samples were reduced for only 1 h (35). In Figure 6.3a, some H_2 generation was observed from TiO_2, but the amount is an order of magnitude lower than that of TiO_2 with metals. This confirms the generally recognized fact that noble metals catalyze the reduction of TiO_2 to Ti_4O_7.

Table 6-8

H_2 Chemisorption on Fresh Catalyst Samples at 300K

Catalyst	Metal Loading μmole/g Catalyst	H_2 Chemisorption, μmole H_2/g Catalyst	
		Reduced at 473K	Reduced at 773K
0.23% Rh/TiO_2	22.3	1.56	0.33
0.45% Pt/TiO_2	23	1.15	0.46
3.7% Ni/TiO_2	628	2.65	0.31

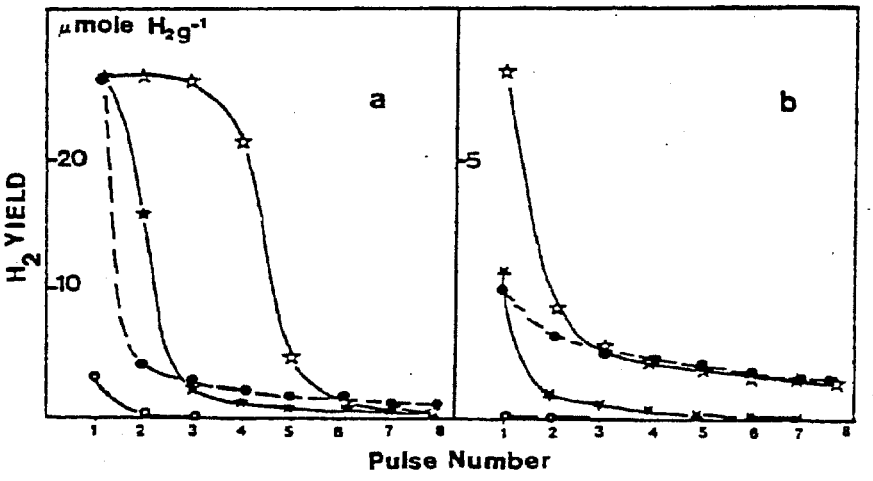

Figure 6-3. H_2 Yield from Pulses of Water Injected on Anatase-Supported Metals Reduced at (a) 773K and (b) 473K. One pulse = 27.5 μmole.

Reference: (50)

6.5 PLATINUM ON TITANIUM OXIDE

Baker recently studied the SMSI of Pt on TiO_2 using transmission electron microscopy and electron diffraction analysis (43). A key finding was that Pt clusters under SMSI take on a pillbox-like morphology of hexagonal outline as opposed to a rounded globular morphology in the non-SMSI state. Electron diffraction analysis and high-resolution electron microscopy showed that TiO_2 in contact with Pt is transformed to Ti_4O_7. This lower oxide structure is not present when TiO_2 is subjected to high-temperature reduction in the absence of Pt. Baker postulates that the pillbox morphology of Pt is due to the greater wettability of Ti_4O_7 toward Pt, as compared with TiO_2.

When silver was deposited on the TiO_2 support and reduced in H_2 at 550°C, an electron micrograph of silver showed a globular outline. The support remained unchanged. Introduction of Pt onto the same catalyst and reduction brought about massive changes in the characteristics of the silver crystallites and the support. Silver particles were no longer globular, but were pillbox shaped. The support was transformed to Ti_4O_7. These observations suggest that Pt acts as a source of H atoms, converting TiO_2 to Ti_4O_7.

The above experiment is interesting in two respects. One is the lowering of the reduction or SMSI temperature, and the other is the induction of morphological changes on silver particles by Pt. These effects are unique areas of multimetallic catalyst research that have not been explored to any significant extent.

In a forerunner to the above paper, Baker described more details of the series of SMSI tests involving Pt on TiO_2, SiO_2, Al_2O_3, and graphite (45). For the electron microscopy work, he prepared approximately 35-nm films of titanium oxide, aluminum oxide, and silicon oxide by sputtering the respective target materials onto rock salt crystals. The rock salt was subsequently dissolved in water, leaving the oxide films floating on the surface. Sections of the films were then picked up on 200-mesh stainless steel electron microscope grids. Carbon films of a similar thickness were prepared by vacuum deposition from a carbon arc onto a Pyrex slide that had been previously coated with a film of

detergent. The resulting carbon film was released from the slide by gradual immersion in water and finally mounted on a microscope grid.

Platinum was evaporated at 10^{-6} torr onto these supports from a spectrographically pure platinum wire. This procedure produced a platinum film approximately one atom thick. Specimens were subsequently reduced in a 20% H_2/80% He mixture for 1 h at 425K, 825K, 975K, and 1075K. After cooling, they were examined in a transmission electron microscope with a resolution better than 0.25 nm. Particle size distributions were obtained from measurement of over 600 particles after each H_2 treatment.

Starting at 425K and continuing to 1075K, a blank titanium oxide in H_2 undergoes changes from the original amorphous structure to a more crystalline form. Electron diffraction patterns of the 1075K sample taken at selected areas were those of the rutile form of TiO_2.

With Pt dispersed over its surface, TiO_2 underwent the same crystallization process observed for the blank titanium oxide. But after reduction at 825K, the structure was that of Ti_4O_7 rather than the rutile form of TiO_2.

Pt particles on the support films undergo changes as they are subjected to the reduction treatments. The Pt particle size distributions are shown in Figure 6-4 (titanium oxide), Figure 6-5 (aluminum oxide), Figure 6-6 (silicon oxide), and Figure 6-7 (carbon).

The distribution on TiO_2 is narrower than for the other substrates at all temperatures and shows little change in magnitude over the range 825K to 1075K. The mean particle size on TiO_2 is about 3 nm at 425K and increases slowly to about 6 nm at 1075K. Particle growth for the other supports is greater, particularly on silica and graphite.

The particle size distributions as a function of reduction temperature give further evidence of the SMSI of Pt on TiO_2. The fact that unusually narrow distribution of small Pt particles is retained on TiO_2 even to 1075K points to

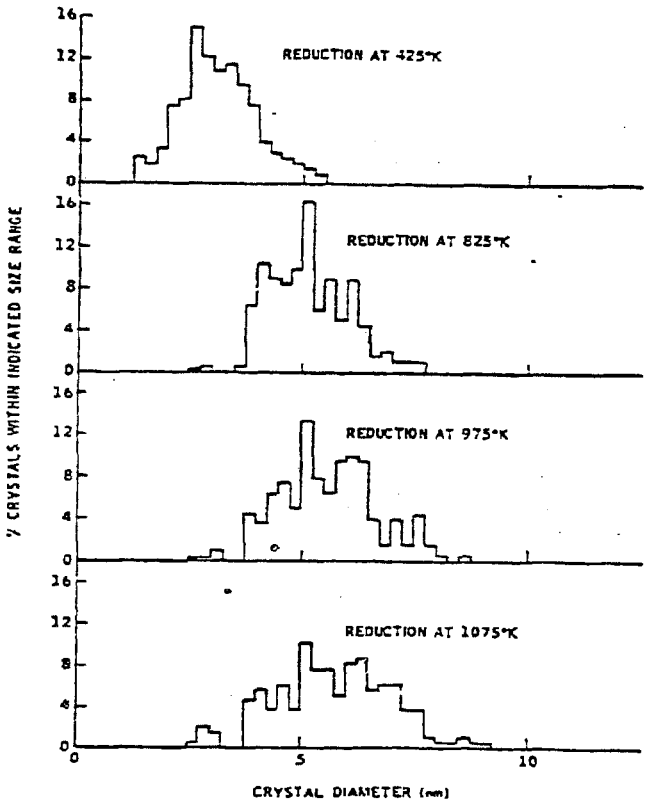

Figure 6-4. Variation of Particle Size Distribution with Reduction Temperature for Pt on Titanium Oxide

Reference: (45)

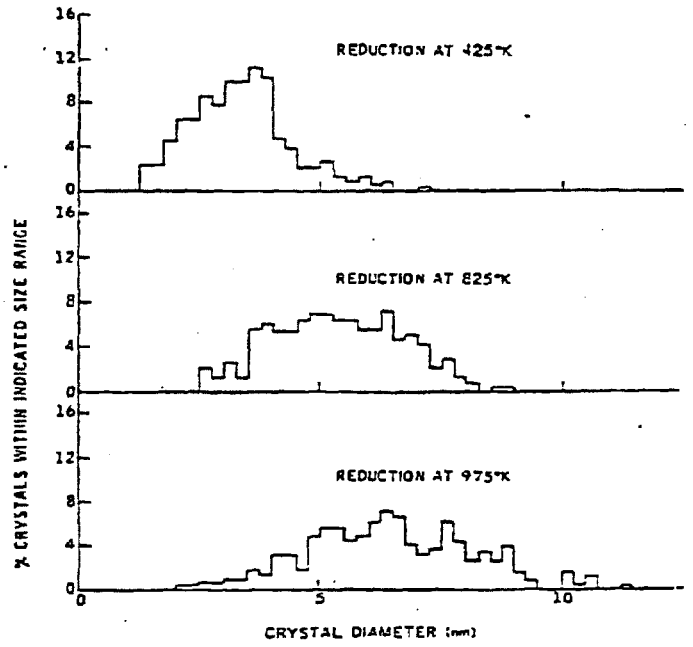

Figure 6-5. Variation of Particle Size Distribution with Reduction Temperature for Pt on Aluminum Oxide

Reference: (45)

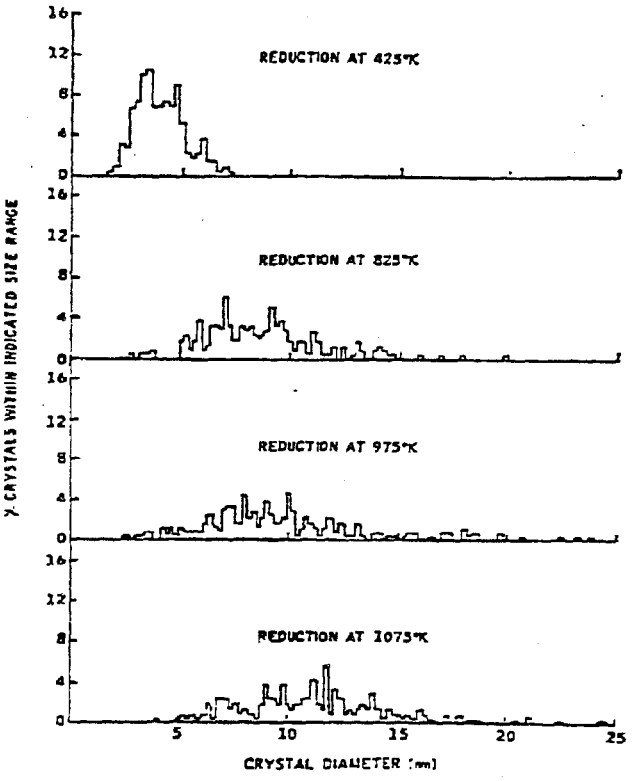

Figure 6-6. Variation of Particle Size Distribution with Reduction Temperature for Pt on Silicon Oxide

Reference: (45)

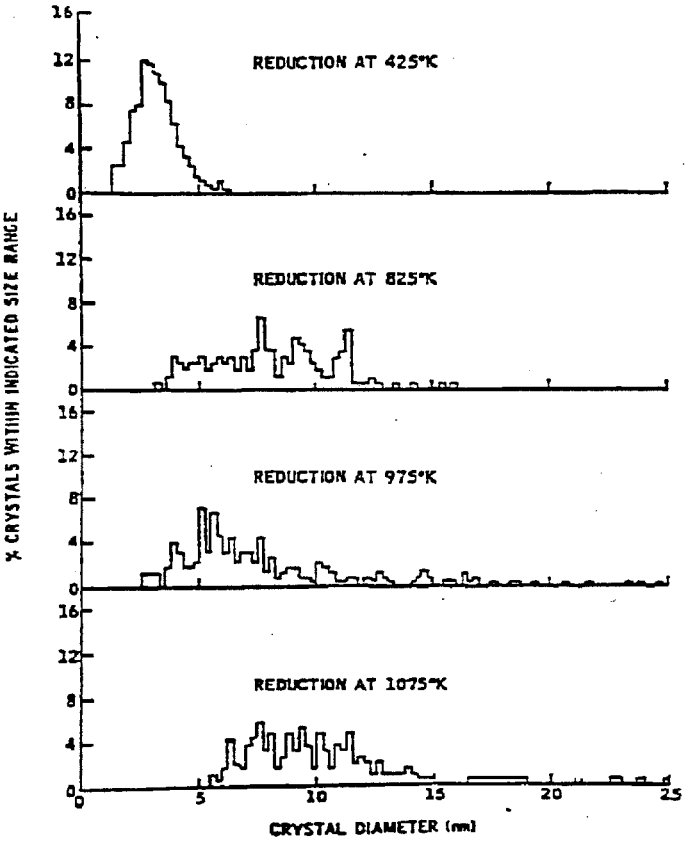

Figure 6-7. Variation of Particle Size Distribution with Reduction Temperature for Pt on Carbon

Reference: (45)

the presence of metal-support bonding, inhibiting the usual sintering by atomic or particle migration.

Pt particles on TiO_2 under SMSI retain a narrow size distribution, as shown in the above work, but when SMSI is reduced or eliminated by oxidation with H_2O or O_2, the size distribution becomes much broader. This has been demonstrated by Baker (49) in a follow-up paper to the work cited above (43). The sample film preparation for electron microscopy and particle size distribution measurements is the same in both papers.

In the second study, Pt on TiO_2 film was treated under various amounts of pressure. The results are shown in Figure 6-8.

The nature of Pt particles after reduction at 875K (Figure 6-8a) was identical to that reported in the preceding paper (43), having the form of thin hexagonal pillboxes. The particle size distribution was also identical. However, subsequent treatment with water vapor at 525K brought an appreciable increase in the particle size (Figure 6-8b). Treatment with oxygen (Figure 6-8c) caused a more dramatic agglomeration, resulting in a broadening of the particle size from a 2-8 nm range for the sample before H_2O/O_2 treatment to a 3-18 nm range after treatment.

After H_2O treatment in Step B, the sample was reduced in H_2 at 875K for 1 hr before Step C. Therefore it is not clear whether the agglomeration was the result of H_2 reduction or O_2 oxidation. Some clues may be found in Step D, where the oxidized form of the sample from Step C was again exposed to H_2 at 875K. the oxidized form of the sample from Step C was again exposed to H_2 at 875K. Here it can be seen that a significant number of the large particles in Step C were disproportionated to smaller fragments. The fragmentation creates particles that are much smaller than those that existed on the fresh sample.

Electron diffraction examination demonstrated that the H_2 reduction in Steps A and D tranformed the support to Ti_4O_7, while after oxidation in either H_2O or O_2, it was TiO_2.

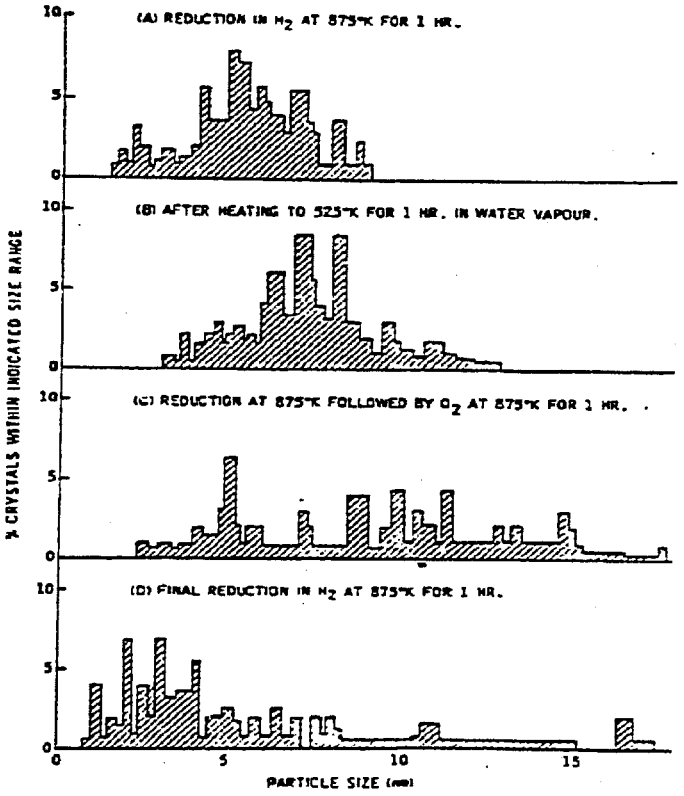

Figure 6-8. Particle Size Distribution of Pt Crystallites After Consecutive Treatments in Various Environments

Reference: (49)

6.6 RHODIUM ON TITANIUM OXIDE

Resasco prepared 2 wt% Rh/TiO_2 samples of varying dispersion and tested them for alkane hydrogenolysis after low-temperature (523K) and high-temperature (773K) reduction (44). The results for ethane, n-butane, and cyclohexane hydrogenolysis are shown in Figure 6-9, Figure 6-10, and Figure 6-11, respectively. Figure 6-11 includes cyclohexane dehydrogenation.

The key findings of this study are the following:

- The samples reduced at high temperature show poor activities toward all hydrogenolysis reactions.
- For low-temperature samples, the hydrogenolysis activity increases or stays constant with increasing metal dispersion. For high-temperature samples, the activities decrease sharply with increasing dispersion.
- While high-temperature reduction reduces cyclohexane hydrogenolysis, it does not affect the cyclohexane dehydrogenation.

All activities are given in terms of exposed Rh atoms measured by H_2 chemisorption on the samples reduced at low temperature. The possibility of Rh sintering during the high-temperature reduction was rejected, based on work by Baker that showed the dispersion of Pt on TiO_2 to be stable in that temperature range (45). In the absence of data for Rh, this may be a reasonable assumption. Thus, the observed activity losses in hydrogenolysis are mose likely due to SMSI.

6.7 SMSI in CO/H_2 REACTIONS

Vannice investigated hydrocarbon synthesis from CO/H_2 over several supported catalysts and found that SMSI of Ni/TiO_2 enhances the formation of C_2 and hydrocarbons (42). The H_2 and CO chemisorption and CO/H_2 reaction for various supported nickel catalysts were measured, and the results are shown in Table 6-9.

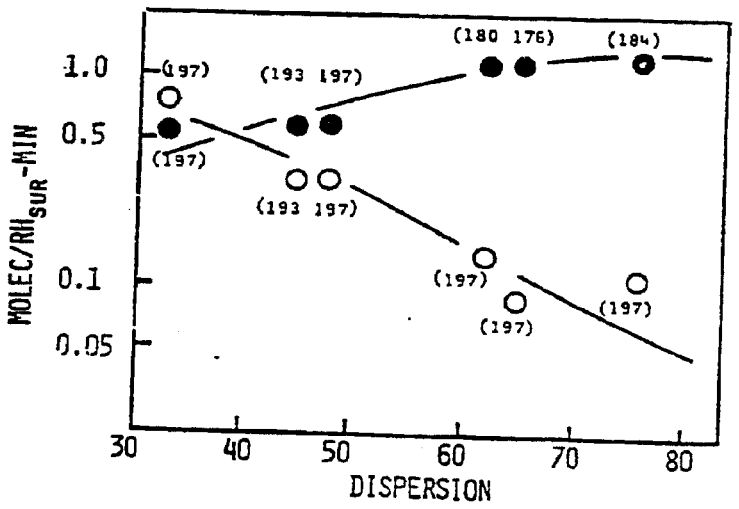

Figure 6-9. Ethane Hydrogenolysis as a Function of Dispersion. The number in parentheses by each point is the apparent activation energy in units of kJ/mol. The rates were measured at 523K (•) for low-temperature reduction and 623K (o) for high-temperature reduction.

Reference: (44)

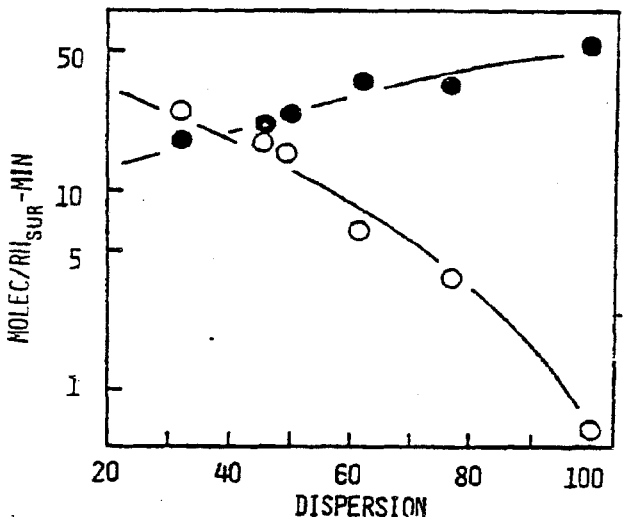

Figure 6-10. n-Butane Hydrogenolysis as a Function of Dispersion. The rates were measured at 473K (●), for low-temperature reduction and at 573K (o) for high-temperature reduction.

Reference: (44)

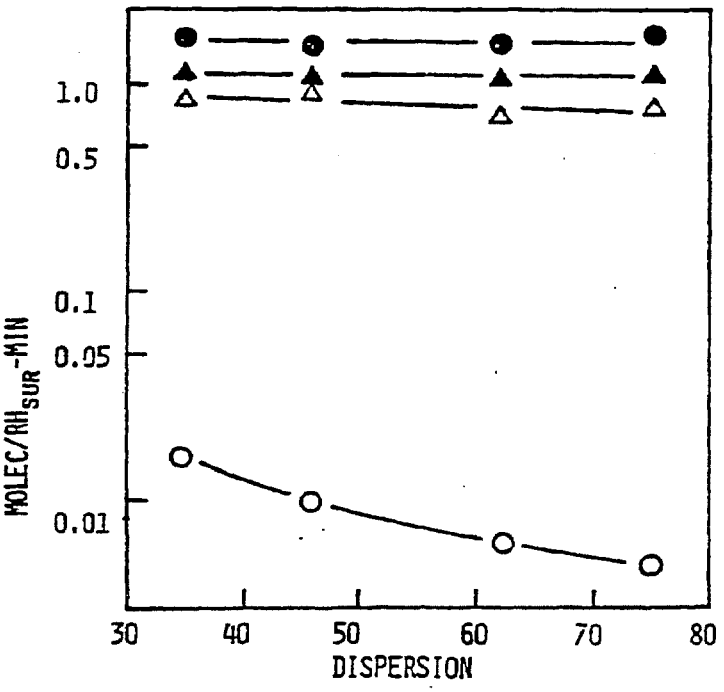

Figure 6-11. Cyclohexane Hydrogenolysis (o)/Dehydrogenation (Δ) as a Function of Dispersion. The rates were measured at 573K for both low-temperature reduction (solid) and high-temperature reduction (open).

Reference: (44)

Table 6-9

H_2 Chemisorption and CO/H_2 Reaction on Ni Catalysts

	Chemisorption		CO/H_2 Reaction							
			CO Conversion[a],	Product Analysis, mole %[b]						
	H Atoms/Ni Atom	CO Atoms/Ni Atom	moles/sec/g Ni	Temp, K	CO Conversion, %	C_1	C_2	C_3	C_4	C_{5+}
1.53% Ni/TiO_2	0.032	0.15	8.35	524	13.3	58	14	12	8	7
10% Ni/TiO_2	0.056	0.076	22.8	516	24	50	9	25	8	9
5% Ni/η-Al_2O_3	0.27	0.28	3.44	527	10.8	90	7	3	1	-
8.8% Ni/η-Al_2O_3	0.30	-	1.63	503	3.1	81	14	3	2	-
42% Ni/α-Al_2O_3	0.034	0.050	0.21	509	2.1	76	1	5	3	1
16.7% Ni/SiO_2	0.27	-	2.36	493	3.3	92	5	3	1	-
20% Ni/graphite	0.022	0.003	0.064	507	24.8	87	7	4	1	-
Ni powder	0.0021	0.0031	0.032	525	7.9	94	6	-	-	-

[a]Reaction conditions: 478K, 103 kPa (1atm), $H_2/CO = 3$

[b]Reaction conditions: 103 kPa (1atm), $H_2/CO = 3$

Reference: (42)

For similar Ni loadings, 10% Ni/TiO_2 showed a much lower H_2 chemisorption activity than did 5% $Ni/n\text{-}Al_2O_3$ or 8.8% $Ni/n\text{-}Al_2O_3$. This may be due to SMSI but may also be due to the availability of fewer Ni surface atoms. This is because the BET surface area of TiO_2 is usually five to six times lower than that of the other supports listed in Table 6-9 and larger Ni particles may be expected from the TiO_2 samples. X-ray diffraction measurements of 10% Ni/TiO_2 samples showed the presence of Ni particles.

The chemisorption and x-ray diffraction measurements did not offer convincing evidence of SMSI for Ni/TiO_2, but studies of activity and selectivity in the CO/H_2 reaction give evidence of SMSI. This is shown in Table 6-9. First, the CO conversion per gram Ni is unusually high for 10% Ni/TiO_2. This is rather impressive from a standpoint that the active metal was on a low-surface-area support and therefore the surface-to-bulk ratio would be lower than with the other supports. Second, the product distributions for both 1.53% and 10% Ni/TiO_3 are clearly different. These two catalysts made about one-half as much methane as the other catalysts did.

Another sign of SMSI of the Ni/TiO_2 was the suppression of nickel carbonyl formation. This was demonstrated between a 10% Ni/TiO_2 and a 10% Ni/SiO_2. After reduction with H_2 at 500°C and cooling to room temperature, both samples were contacted with carbon monoxide, and nickel carbonyl vapor was monitored by infrared spectroscopy. The results are shown in Figure 6-12. Nickel carbonyl is immediately detected with Ni/SiO_2, whereas it was not detected for Ni/TiO_2 until 1 h later, and only in a much lower concentration. Clearly, carbonyl formation on the TiO_2 support is severely inhibited, with SMSI being the likely cause.

NiO on supports cannot be reduced at 200°C as was possible with the noble metals tested by Tauster (see Section 6.2); thus, Ni/TiO_2 without SMSI cannot be prepared by the conventional preparation steps involving impregnation, calcination, and reduction.